PNAS RESEARCH ARTICLE | BIOPHYSICS AND COMPUTATIONAL BIOLOGY

Skin wrinkles and folds enable asymmetric stretch in the elephant trunk

Andrew K. Schulz[a], Madeline Boyle[a], Colin Boyle[b], Sophia Sordilla[a], Catalina Rincon[a], Scott Hooper[c], Catie Aubuchon[c], Joy S. Reidenberg[d], Claire Higgins[b], and David L. Hu[a,e,1]

Edited by David Weitz, Harvard University, Cambridge, MA; received December 28, 2021; accepted May 15, 2022

The elephant's trunk is multifunctional: It must be flexible to wrap around vegetation, but tough to knock down trees and resist attack. How can one appendage satisfy both constraints? In this combined experimental and theoretical study, we challenged African elephants to reach far-away objects with only horizontal extensions of their trunk. Surprisingly, the trunk does not extend uniformly, but instead exhibits a dorsal "joint" that stretches 15% more than the corresponding ventral section. Using material testing with the skin of a deceased elephant, we show that the asymmetry is due in part to patterns of the skin. The dorsal skin is folded and 15% more pliable than the wrinkled ventral skin. Skin folds protect the dorsal section and stretch to facilitate downward wrapping, the most common gripping style when picking up items. The elephant's skin is also sufficiently stiff to influence its mechanics: At the joint, the skin requires 13 times more energy to stretch than the corresponding length of muscle. The use of wrinkles and folds to modulate stiffness may provide a valuable concept for both biology and soft robotics.

hydrostat | biomechanics | biomaterials | bioinspired design

Significance

Muscular hydrostats such as octopus arms and the elephant trunk have received much attention because of their dexterity in grabbing a wide range of objects. These animals have inspired soft-robotic manipulators and actuators with various applications, from working with humans in disaster relief to picking up fruit. For soft robots to apply large forces, they will need a protective skin. This work shows that wrinkles and folds in skin can provide protection and flexibility to soft appendages. We hope this work will inspire future work in the mechanics of skin in both animals and robots.

Standing with its shoulders up to 4 m tall, the African elephant relies on its 1.5-m-long trunk to manipulate objects. The trunk is flexible enough to reach down to the ground (grazing) or up into a tree (browsing). Like the human hand that grips objects with its palm, the trunk is prehensile and grips objects with its ventral surface. The trunk's tough dorsal side faces the elements and headbutts trees and predators. In this investigation, we study how the dorsal and ventral skin affect the elephant trunk's mobility.

Elephant trunks have long been an inspiration for soft robots (1–7), which are flexible devices envisioned to provide gentle contact with humans and fragile objects like fruit. Many soft robots are driven by elastomerics and inflatable bladders powered by hydraulics or pneumatics, all of which are easily damaged by sharp objects. Due to their material makeup, soft robots generally have payloads of less than a few kilograms (8), limiting their use. To provide strength without limiting flexibility, several approaches have been attempted. Inspired by the flexible dermal armor of the pangolin and armadillo (9), a wearable skin-interfaced device has been built that consists of an underlying compliant layer covered by stiff tessellated outer plates (10). In another design, a tough elastomer self-heals accumulated scratches at room temperature (11). Kirigami skin has also been designed for use in locomotion and proprioception of soft robots (12, 13).

Unlike musculoskeletal systems with bones and joints, an elephant trunk is flexible because it is a muscular hydrostat: a boneless structure composed of densely packed muscle fibers wrapped in skin (14). Examples of such organs are found everywhere in nature where extreme flexibility is needed, from mammalian and chameleon tongues to octopus arms. The various orientations of the muscle fibers provide opposition enabling various movements including roll, pitch, and yaw. The largest muscular hydrostats in the world include the blue whale tongue, which can weigh up to 2,600 kg (15), and the giant squid tentacle, which can measure 12 m in length (16).

The skin of the elephant has long drawn attention for its permanently wrinkled appearance, a feature shared with naked mole rats and Chinese Shar-pei dogs. In the late 1700s, elephants were originally classified as "pachyderms," meaning animals with thick skin. Indeed, an African elephant weighing 3,500 kg has a measured skin surface area of $A = 20.7\ \mathrm{m}^2$ (17), which is around 10 times the human surface area of skin, $2.04\ \mathrm{m}^2$. Like the skin of all mammals, elephant skin acts as a physical and immune barrier, blocking environmental agents such as viruses, bacteria, ultraviolet light, and toxins. Elephant skin also protects the body against minor cuts and abrasions and has lost its sweat glands to reduce water loss. When elephants cover themselves with mud, their skin wrinkles hold in the moisture to keep them cool (18). African elephants are more wrinkled and have

Author affiliations: [a]George W. Woodruff School of Mechanical Engineering, Georgia Institute of Technology, Atlanta, GA 30332-0405; [b]Department of Bioengineering, Imperial College London, London SW7 2BX, United Kingdom; [c]Department of Elephants, Zoo Atlanta, Atlanta, GA 30318; [d]Center for Anatomy and Functional Morphology, Icahn School of Medicine at Mount Sinai, New York, NY 10029-6574; and [e]School of Biological Sciences, Georgia Institute of Technology, Atlanta, GA 30332-0405

Author contributions: A.K.S., C.B., S.H., C.A., J.S.R., C.H., and D.L.H. designed research; A.K.S., M.B., C.B., S.S., C.R., S.H., C.A., and J.S.R. performed research; A.K.S., S.H., C.A., J.S.R., C.H., and D.L.H. contributed new reagents/analytic tools; A.K.S., M.B., C.B., S.S., and C.R. analyzed data; and A.K.S., M.B., J.S.R., C.H., and D.L.H. wrote the paper.

The authors declare no competing interest.

This article is a PNAS Direct Submission.

[1]To whom correspondence may be addressed. Email: hu@me.gatech.edu.

This article contains supporting information online at https://www.pnas.org/lookup/suppl/doi:10.1073/pnas.2122563119/-/DCSupplemental.

Published July 18, 2022.

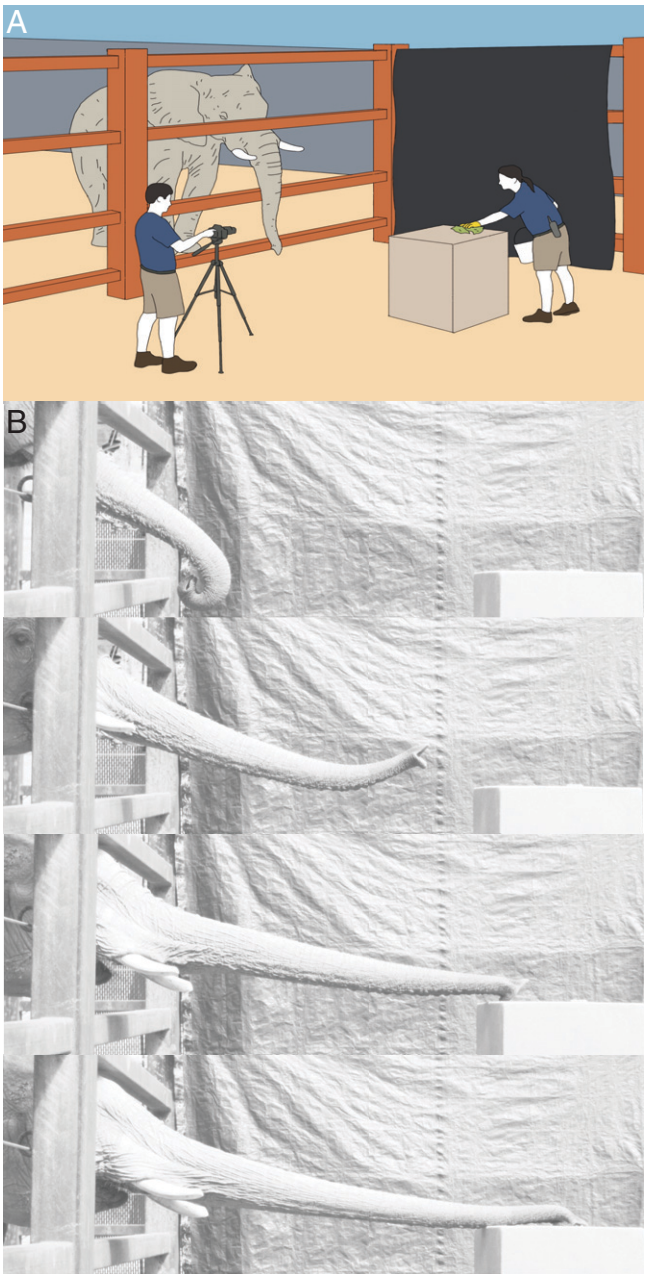

Fig. 1. (*A*) The experimental setup for studying elephant trunk elongation. Illustration done by B. Seleb. (*B*) A time series of the male elephant reaching for a food item. Images are separated by 0.33 s.

larger ears than Asian elephants due to their different climate. Elephants and seals cool themselves with highly vascularized skin regions called thermal windows, which emanate heat much more than the rest of the body (19). While elephant skin has been shown to have a role in thermal regulation, we show here that it also plays a mechanical role in enabling trunk mobility.

Results

We observed a male African elephant and a female African elephant elongating their trunks to reach food items placed at a set horizontal distance (Fig. 1*A*). Ten trials were conducted with the female elephant, with 7 reported here; another 5 trials were conducted with the male elephant, with 3 reported here. Unusable trials involved the elephant grabbing the tarp or failing to reach. Henceforth, averages and SDs are calculated across n trials for a single elephant, where n is stated in each instance. Since we had access to only one elephant of each sex, we did not make any statistical comparisons between the sexes.

The reaching movement may be divided into three phases: hanging, lifting, and elongation (Fig. 1*B*). When the elephant was resting, its trunk's hanging length was 126 cm for the female and 141 cm for the male. From this baseline length, we will describe the trunk deformation in terms of strain, the ratio of the trunk's change in length to its original hanging length. For example, a strain of 0.2 indicates that the trunk has increased in length by 20% of its hanging length and a strain of –0.2 indicates that it has contracted by 20%. The first stretch occurred when the trunk rose to a horizontal position. During this rise, the elephant trunk strained by 0.20 ± 0.045 ($n = 7$) for the female and 0.12 ± 0.012 ($n = 3$) for the male (*SI Appendix*, Fig. S1). Thus, raising the trunk prepares it for reaching by generating muscular contractions that lengthen it substantially. The trunk elongated farther during the reaching movement, generating a final strain of 0.25 for the female and 0.13 for the male (Fig. 2). Every trial consisted of both lifting and elongation phases, the combination of which had a duration of 2 ± 0.15 s ($n = 10$).

How does the elephant trunk strain compare to other muscular hydrostats? We compiled the maximum observed strain for the hydrostat appendages of 13 species, including chameleon and mammal tongues, octopus arms, and elephant trunks (20–25). Fig. 2 shows the relationship between body mass M and maximum axial strain ε_A. The dashed line shows the power-law best fit of

$$\varepsilon_A = 2.17 M^{-0.245}, \qquad [1]$$

where M is in kilograms and $R^2 = 0.68$ is the log-log coefficient of determination. The power law in Eq. **1** gives interpolated values that generally compare well with experimental measurements. For example, octopuses (9 kg) exhibit a strain of 2.66 (22), which compares closely to the interpolation of 2.57. Female (3,400 kg) and male (4,550 kg) elephants have strains of 0.25 and 0.13, respectively, with interpolations of 0.15 and 0.07. Clearly, strain

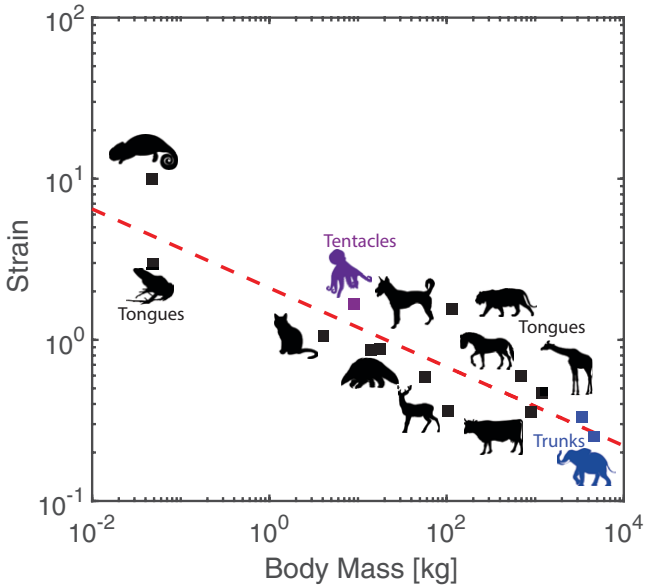

Fig. 2. The relation between maximum strain and body mass for animals possessing muscular hydrostats as appendages (20–25). The tongues are shown by black points, octopus tentacles by the purple point, and the elephant trunks by the blue points. A red dashed line depicts the power-law best fit. Raw data and citations are given in *SI Appendix*, Table S3. Silhouettes are from Adobe stock photos.

decreases with increasing body size, a trend that is even supported across sexes in elephants. One outlier is the chameleon (0.047 kg), which exhibits a strain of 10.0 (20), much larger than the interpolation of 5.37. The chameleon evolved a series of 10 stacked concentric sheaths in its tongue, which enables it to extend like a telescope (20). We can take this idea that larger hydrostats have diminishing stretch to its limit: If muscular hydrostats continued to increase with body size, our power law suggests that an animal of weight 10,000 kg should have a muscular hydrostat incapable of stretching. This weight corresponds to the largest terrestrial mammal that ever lived, the woolly mammoth, estimated between 6 and 7 tons (26). It remains unknown how extinct animals such as dinosaurs, which weighed up to 77 tons, escaped the consequences of the trends above. The theoretical basis for this power law remains unknown, but we list other physical constraints on muscular hydrostats in *Discussion*.

In octopus arms and most mammalian tongues, elongation occurred uniformly across the appendage length (24, 27). However, in elephant trunks, elongation occurred in waves of extension that started at the tip and traveled toward the base. Fig. 3*A* shows the time course of the positions of 14 equally spaced points along the trunk of the female elephant. We show a single trial here, without averaging across other trials, to make clear the characteristics of the traveling wave. Other trials also show the existence of one to two traveling waves. The black line corresponds to the position of the trunk tip, which represents the sum of all the extensions of segments posterior to it. Inflection points mark the onset of extensional waves. As denoted by the black arrows, two waves were generated, one with an onset at $t = 0.4$ s and the other with onset at $t = 1.6$ s (Fig. 3*A*). Presumably, the first wave produced insufficient elongation to reach the object, so the elephant introduced a second wave. Unlike the first wave, the second wave traveled only to the trunk's midpoint, which appears to mark the limit of the trunk's extension.

Both male and female elephants showed at least one peak in strain rate, consistent with the first of the two traveling waves described above. The male elephant had a maximum strain rate of 0.25 s^{-1} occurring at time $t = 0.2$ s. Similarly, the female elephant had a maximum strain rate of 0.2 s^{-1} at a time $t = 0.85$ s (*SI Appendix*, Fig. S2). Squid tentacles also exhibit significant strain rates and oscillatory patterns that are qualitatively similar to those of the elephant trunk (28).

One of the constraints of hydrostatic organs is that they satisfy conservation of mass. Because the volume of the organ is fixed, longitudinal extension must be accompanied by contraction in the lateral direction. This physical picture has been shown to accurately describe appendages such as octopus arms and mammalian tongues, but not yet for the elephant trunk, which contains two hollow nasal passages. We derived the relationship between axial strain (change in length) and lateral strain (change in diameter) in Eq. **10**. Inputs to this model include the internal and external dimensions of the trunk measured using a computerized tomography (CT) scan of a postmortem, previously frozen elephant trunk. Based on the measured axial strain, we predicted the lateral strain for the female elephant, which we compare to experimental values (Fig. 3*B*). Based on the average axial strain along the trunk of 0.199 ± 0.045 ($n = 7$), we calculate a lateral strain of –0.039, which is 0.046 lower in magnitude than the observed value of –0.086 ± 0.043 ($n = 7$). The higher-than-expected lateral strain magnitude may be an error approximating the trunk's cross-section as a circle; in reality, it is round on the dorsal side and flat on the ventral side. Our model shows that the observed lateral strain is consistent with a volume decrease of 0.18 L, which is 0.2% of the trunk volume, a negligible amount. We thus conclude the elephant trunk indeed satisfies conservation of mass.

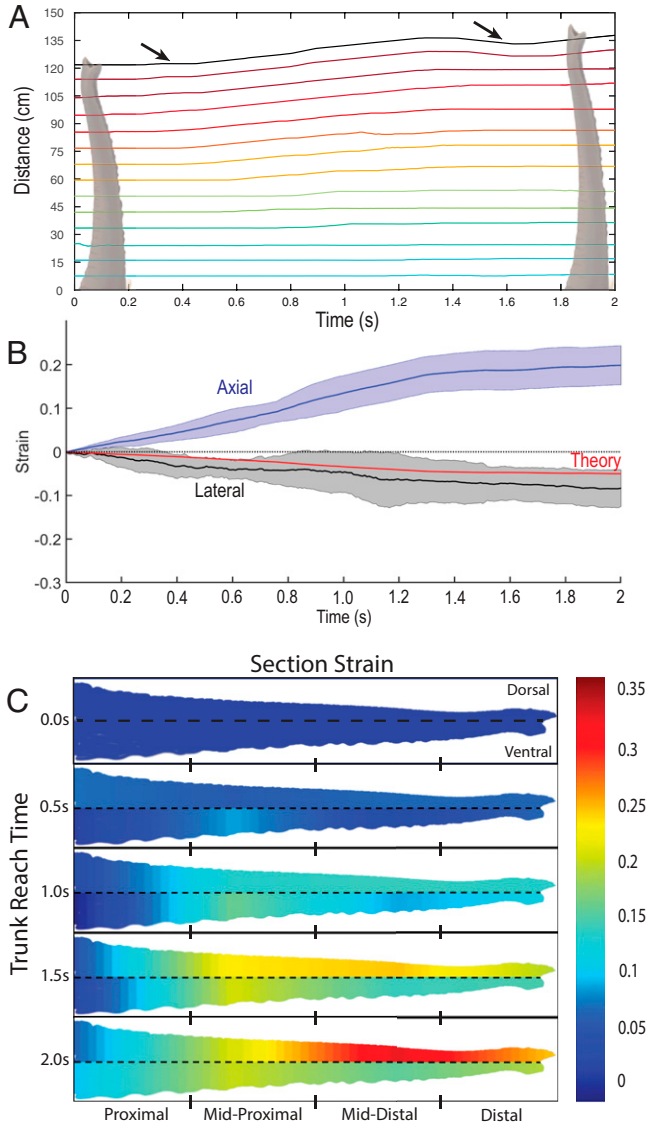

Fig. 3. (*A*) Time course of the positions of 14 equidistant points along the trunk of the female elephant ($n = 1$). The arrows indicate the onset of the waves of extension that travel in the proximal direction. (*B*) Time course of the average strain in the trunk of the female elephant ($n = 7$). The blue line is the average axial strain, and the black line is the average lateral strain, both measured from experiments. The red line is the predicted lateral strain based on volume conservation. The dotted line at zero strain is for reference. (*C*) Time series of the average trunk strain for the dorsal and ventral regions of the female elephant ($n = 7$ trials). The color bar indicates axial strain.

We discovered that the trunk exhibits striking differences in ventral and dorsal strain. To better describe the location of greatest ventral–dorsal disparity, we divide the trunk into four sections of 30-cm length: the proximal, midproximal, middistal, and distal sections. The heat map in Fig. 2*C* shows, at 2 s of elongation, the dorsal middistal part of the trunk (30 to 60 cm from the tip) strained to 0.35, while the corresponding ventral section strained to nearly half the value of 0.18. The anomalous dorsal–ventral strain difference is 0.17, equivalent to an extra displacement of 5.1 cm in the dorsal section. This displacement is substantial when compared to other regions of the trunk, where the difference between dorsal and ventral regions is an order of magnitude less. For example, the proximal region (90 to 120 cm) has dorsal and ventral strains of 1.10 and 1.12, respectively, a difference that corresponds to 0.5 cm.

What is the utility of reaching farther with the dorsal section of the trunk? We first hypothesized the difference in strain was due to the dorsal trunk traveling a curved and thus longer path to reach the target. However, 18 of the 20 horizontally spaced points on the dorsal and ventral regions showed nonsignificant curvature values, as shown by their P values >0.05 (*SI Appendix*, Table S1 and Fig. S3). The only two positions with P values less than 0.05 each had such small curvature values of 0.02 m^{-1} (or equivalent radii of curvature of 50 m) that we can conclude those regions are straight. Moreover, those regions did not correspond to the middorsal section where we observed the asymmetry.

Instead, we conclude that the dorsal trunk tip stretches farther, which helps the trunk tip to pitch forward to reach the object, as shown at $t = 0.95$ s in Fig. 1*B*. The observed asymmetry is not a chance observation, but is a repeatable feature of all trials for both male and female elephants. To seek rationale for the asymmetry, we proceed with observations of trunk skin and muscle anatomy.

The anomalous stretch of the dorsal trunk is consistent with the extensibility of the dorsal skin. Our frozen elephant trunk has dorsal skin composed of a series of folds with overlapping lengths of 4 cm. In contrast, the ventral skin is composed of wrinkles with a smaller length scale of 1 to 2 cm. Fig. 4*C* shows stress–strain measurements of dorsal and ventral skin taken from the proximal trunk base. We observe similar behavior in our elongation experiments. Specifically, dorsal and ventral sections have comparable elasticity in the linear regime, with Young's modulus of 470 ± 15 kPa ($n = 3$) for the dorsal and 483 ± 13 kPa ($n = 3$) for the ventral sections (Fig. 4*C*). The linear regime occurs within strains of 0 to 0.15. This strain regime corresponds closely to the observed strains in our elongation experiments where dorsal and ventral sections align (before the time of 1.0 s in Fig. 2*B*). Above this strain, the differing geometry of the wrinkles and folds influences their elasticity. Indeed, the nonlinear regime of the tensile tests shows that the dorsal region maintains a comparable Young's modulus as its linear regime, 670 ± 65 MPa ($n = 3$), while the ventral region shows a stiffer Young's modulus of

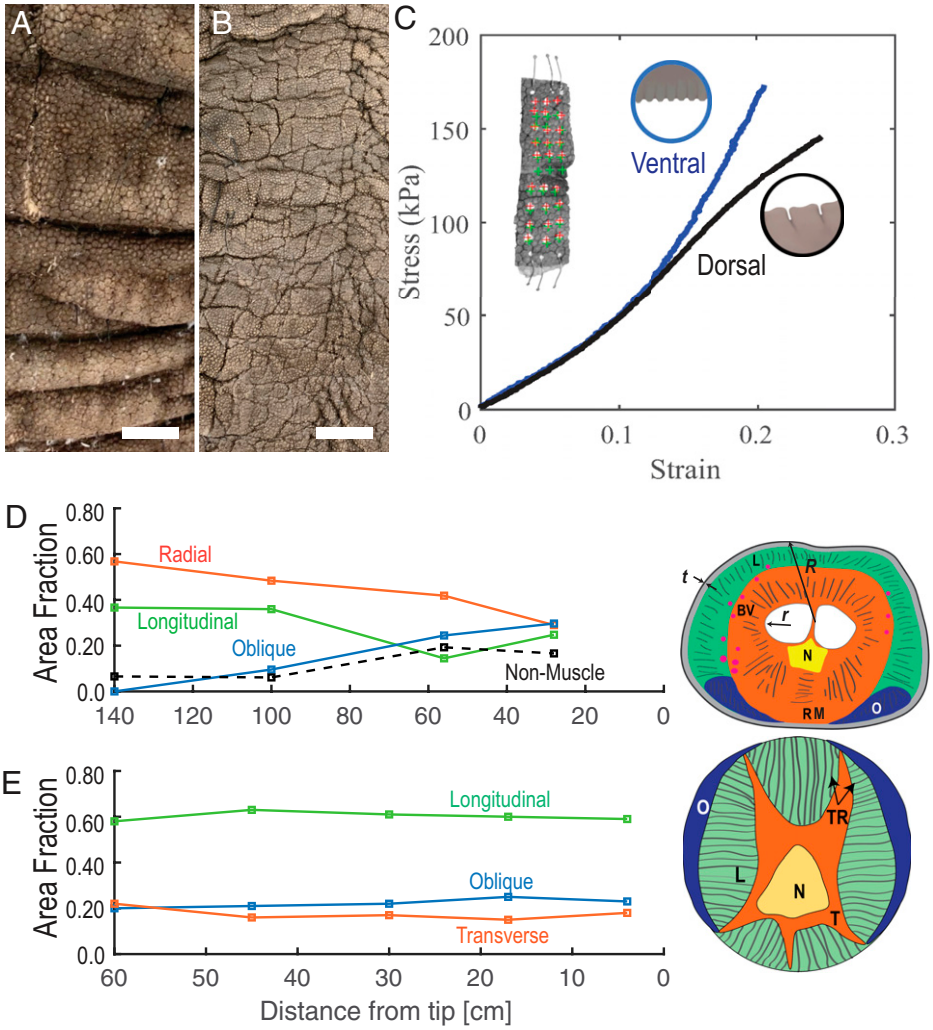

Fig. 4. Elephant trunk skin and cross-section. (*A*) Photographs of skin from dorsal skin of the frozen elephant trunk, taken from the proximal region, 110 cm from the distal tip. (*B*) Ventral skin. The longitudinal axis of the trunk is vertical in the images. The dorsal section is characterized by large folds and the ventral section by clusters of wrinkles. (Scale bar, 1 cm, with the bottom of the images toward the distal tip of the trunk.) (*C*) The stress–strain relationship for the dorsal skin (black) and ventral skin (blue). *Inset* shows how natural features were tracked using Digital Image Correlation. (*D* and *E*) The relationship between the area fraction and distance *z* from the tip for components of (*D*) the frozen female elephant trunk and (*E*) an octopus arm, reprinted from ref. 27. The area fraction is defined as the ratio of the cross-sectional area of the component to the total cross-sectional area. *Insets* show the cross-section of the elephant trunk and octopus arm with the different muscle groups labeled: longitudinal muscle (L) in green, radial muscle (RM) in orange, and oblique muscle (O) in blue. The dashed line indicates nonmuscular areas of the cross-section, which consists of skin, nasal passageway, nerves (N), and blood vessels (BV). Trabeculae connective tissue (TR) is also labeled on the octopus cross-sectional image.

1.19 ± 0.12 MPa ($n = 3$). The ratio of Young's moduli is 1.77, which corresponds closely to 1.75, the ratio of dorsal to ventral strains in the nonlinear regime of the elongation experiments. We thus conclude that trunk elongation in elephants is influenced by the material properties of their skin.

How much can the skin influence the trunk's motion? The trunk muscle stiffness was previously measured to be 938 kPa, making the elephant skin at most 1.27 times stiffer than the muscle tissue (29). If the trunk stretches, the required strain energy in muscle and skin will be proportional to EV, where E is the Young's modulus and V is the volume displaced. Using measurements of the trunk as shown in *SI Appendix*, Fig. S5*A*, we use Eq. **11** to calculate the ratio λ of skin strain energy to muscle strain energy. At a position 20 cm from the tip, the skin has $\lambda = 13.2$ times more strain energy than the corresponding muscle. This surprising result arises because the nostrils dominate the internal volume at the trunk tip, which increases the ratio of skin to muscle volume (*SI Appendix*, Fig. S5*B* and *C*). Conversely, at a position 110 cm from the tip of the trunk, the skin has only 0.36 the strain energy of the muscle because the nostrils occupy a much smaller fraction of the cross-section. These calculations explain why we observe asymmetry at only one location, near the tip, and not near the base. We note that these are only estimates since muscle tissue can stiffen when contracted.

The trunk's stretch asymmetry is consistent with its internal anatomy. Fig. 4*D* shows the proportions of the three types of muscle as a function of distance from the tip of the trunk: longitudinal muscle (green), radial or transverse muscle (orange), and oblique muscle (blue). For completeness, we also include the dashed line, which accounts for the nonmuscular components of the trunk, such as the nasal cavity, nerves, skin, and blood vessels. Oblique muscles, used to generate left–right yaw motions of the trunk, are found only in the ventral region, with increasing proportion, from 0% at the base to 25% at the tip (Fig. 4*D*). Although yaw motion is not present during uniaxial elongation, the presence of oblique muscles in the ventral section may limit extension, particularly in the middistal to distal sections, where the oblique muscles are the largest proportion of the cross-section. The asymmetric distribution of oblique muscles appears unique to the elephant trunk. As shown in Fig. 4*E*, other hydrostatic organs, such as the arms of the octopus *Octopus bimaculoides*, are generally radially symmetric. Moreover, the proportion of longitudinal, transverse, and oblique muscles is constant from base to tip, ∼60%, 20%, and 20%, respectively (30).

Discussion

In this work, we showed that the elephant's skin can influence its ability to extend the trunk. It is possible that the skin may influence motion at other points on the elephant's body as well. On the elephant's body, the skin thickness, t, is around 10 times that of human skin (1.5 mm) (18). Assuming elephant skin has the same density as human skin, $\rho = 1.02$ g/cm^3 (31), we can approximate the total weight of elephant skin. Given a 3,500-kg elephant's skin area of $A = 20.7$ m^2 (17), the elephant skin weighs approximately $\rho tA = 320$ kg, which is about the weight of a V8 engine. Thus, elephant skin comprises 9% of the elephant's body weight, comparable to human skin, which comprises 10 to 20% of body weight (32). Similar to the trunk, we would expect the skin to affect mobility in any location for which the cross-sectional area of the muscle is small, such as the tail and ears.

It remains unknown why the elephant trunk and chameleon tongue elongate telescopically but the octopus arm elongates uniformly. Telescopic elongation may reduce energy use for elephants because of the trunk's tapered shape. The distal quarter of the trunk contains 1 L of muscle, while the proximal quarter contains 22 L of muscle. The energy expended is proportional to the change in volume for each section. If each section extended the same distance, the proximal trunk would expend 22 times more energy than the distal trunk. Thus, it makes sense that the trunk would only recruit larger cross-sectional areas if necessary. Surprisingly, we saw that muscular hydrostat exhibits power-law trends in elongation with respect to body size. One reason for this is because of trade-offs between stretching and bending. A larger proximal cross-section may limit stretch, but helps the trunk to resist bending due to gravity. Tree branches and other cantilever structures have diameters proportional to their lengths to the 2/3 power, demonstrating a scaling pattern of elastic similarity (33). Careful measurements of elephant trunks across body sizes would be needed to see whether they are also elastically similar.

The chameleon tongue may have evolved telescoping motion to increase the accuracy of striking a target (34). Chameleons unsheathe the 10 stacked muscle layers in their tongue to reach far-reaching objects (20). In addition to chameleon tongues, telescopic behaviors have also been observed in honey bee abdomens, specifically during bending. A flexible membrane allows for each segment of the abdomen to telescope into the next segment (35).

There still remains much to be studied about the traveling waves in the elephant trunk. While the tip of the trunk travels at a speed of 50 cm/s, the wave speed of displacement travels a distance $L = 80$ cm in $\tau = 0.8$ s, indicating a wave speed $u = L/\tau$ of 1.0 m/s. When an elastic material is hammered, the speed of the propagating elastic wave equals the speed of sound in the material, $c = \sqrt{E/\rho}$, where $E = 938$ kPa is the modulus of elasticity of the elephant trunk muscle and $\rho = 1{,}180$ kg/m^3 is its density (29). The elastic wave speed is thus $c = 0.9$ m/s, comparable to the elephant's wave speed of displacement, suggesting that the elephant may be sending traveling waves near the limits that elastic waves can travel through the material. These material wave speeds are small compared to the speed of nerve conduction, which is 70 m/s in an elephant's legs, but has never been measured in the trunk (36). These wave speeds are fast compared to those of snakes, which also send traveling waves during rectilinear motion. For example, Dumeril's boa travels at a body speed of 0.2 to 6 cm/s with a wave speed of 25 cm/s (37).

Using observations of the outside of the trunk, and assuming the nasal cavity remains fixed in size, we concluded that elephant trunks satisfy conservation of mass. Verifying our assumption would require simultaneous measurements of nasal cavity volume. In a previous study of elephants suctioning water–bran mixtures, we found that elephants can contract their trunk muscles to increase their nostril radius by 30% (38). It has long been assumed that there is "no evidence of major fluid flow into [muscular hydrostats]" (39), but future work using ultrasound or other imaging techniques is needed to see whether any nasal cavity expansion occurs during reaching.

The presence of a flexible "joint" in the middistal region helps the ventral and dorsal sections of the trunk to accomplish different functions, as if the elephant had two separate trunks. The dorsal trunk provides sun protection, cushioning when pushing tree trunks, and impact protection during fights with competing elephants or predators such as lions. Moreover, an elephant body skin has been documented to have thick outer cracked layers to allow water propagation through the skin (18). These cracks assist with the distribution of water for thermoregulation and protection from pests.

In comparison, the ventral trunk is used to manipulate different objects (40). It needs a high friction coefficient to maximize

gripping forces and sensitivity to recognize whether an object is slipping. Elephants commonly use their ventral trunk to wrap around and carry food items. The trunk's ventral wrinkles may increase friction similar to wrinkles in the palms of human and primate hands (41). It has been shown that the elephant has a nearly perfect success rate in lifting a range of geometries and sizes of objects when using the distal tip of the trunk (40). Furthermore, elephants rarely utilize the dorsal portion of their trunk for gripping or wrapping (40).

The different functions of dorsal and ventral surfaces are shared with many other hydrostats. Octopus arms have suction-cup grippers only on the ventral side (42). Cat tongues have papillae only on their dorsal tongue, which they use to distribute saliva on their fur. Penguins have spines only on their dorsal tongue, which allow them to better grip and swallow slippery fish (24, 43). Future work may also show that such structures limit movement, as we observed here with the elephant.

Conclusion

Elephants can extend their trunk 10 to 20% to reach faraway objects. Reaching proceeds telescopically, with one to two extensional waves sent from the distal tip to the proximal base. We discovered the presence of a dorsal joint that is more flexible than the corresponding ventral section. The trunk's dorsal and ventral regions extend uniformly in the first half of the reaching task. In the second half of the task, the dorsal middistal section continues to stretch 15% while the corresponding ventral section remains a fixed length. This asymmetry in stretch corresponds closely to the material behavior of the skin, which we studied using tensile tests of a frozen elephant trunk. In this independent test, we found that at high strains, the ventral section is 1.77 times stiffer than the dorsal section. This increased stiffness can restrict trunk motion at the distal tip, where the nostrils take up much of the cross-sectional area.

Mathematical Modeling

Conservation of Volume. We seek to determine the relationship between axial and lateral strain for an elephant trunk satisfying conservation of mass. In reality, the trunk is round on the dorsal side and flat on the ventral side, but for simplicity, we model each segment of the trunk as a conical frustum (truncated cone). The axial strain ε_A of a trunk section is defined as the ratio of the change in length of the trunk δL to its original length L,

$$\varepsilon_A = \frac{\delta L}{L}. \quad [2]$$

Similarly, the transverse strain ε_T is defined as the ratio of the change in radius of the trunk δR to the original radius R,

$$\varepsilon_T = \frac{\delta R}{R}. \quad [3]$$

Conservation of volume (14) states $\delta V \approx 0$, where V is the volume of a conical frustum with axial length L. This may be written as

$$V = \frac{\pi L}{3}[(R_L^2 + R_L R_0 + R_0^2) - 2(r_L^2 + r_L r_0 + r_0^2)], \quad [4]$$

where R_i and r_i are the outer diameter and inner nasal diameter of the trunk, where i denotes the position at either $z = 0$ or $z = L$. We assume that the nasal diameter stays constant during elongation: $\delta r \approx 0$.

Taking the derivative of both sides of Eq. **4** and applying the conservation of volume assumption, $\delta V = 0$, we find

$$\frac{\delta L}{L} = -\frac{\delta\alpha - 2\delta\beta}{(\alpha - 2\beta)}, \quad [5]$$

where $\alpha = (R_L^2 + R_L R_0 + R_0^2)$ and $\beta = (r_L^2 + r_L r_0 + r_0^2)$. Since the nasal diameter stays constant, $\delta\beta \approx 0$. Moreover, we use the definition of axial strain in Eq. **2** to rewrite the axial strain as

$$\varepsilon_A = -\frac{\delta\alpha}{(\alpha - 2\beta)}. \quad [6]$$

In taking the derivative of α, we assume that the elephant trunk tapers uniformly: We introduce a constant c that relates the proximal outer radius to the distal outer radius; where $R_0 = cR_L$ we may write $\delta R_0 = c\delta R_L$. From trunk dissections, we find $c = 1.034$. This allows us to write the derivative of α,

$$\delta\alpha = \delta[(R_L^2 + cR_L^2 + c^2 R_L^2)] = 2R_L\delta R_L(1 + c + c^2), \quad [7]$$

and substitute this expression into Eq. **6**, finding

$$\varepsilon_A = -\frac{2R_L(1 + c + c^2)\delta R_L}{(1 + c + c^2)R_L^2 - 2\beta}. \quad [8]$$

Multiplying the right side of this equation by $\frac{R_L}{R_L}$ allows us to substitute for the transverse strain, further simplifying into

$$\varepsilon_A = -\frac{2R_L^2(1 + c + c^2)\varepsilon_T}{(1 + c + c^2)R_L^2 - 2\beta}. \quad [9]$$

Finally, solving this equation for the transverse strain and substituting the value for β, we find

$$\varepsilon_T = -\varepsilon_A\left(\frac{1}{2} - \frac{r_0^2 + r_L r_0 + r_L^2}{R_L^2(c^2 + c + 1)}\right). \quad [10]$$

Energy Ratio. Here we use the trunk's shape and material properties to calculate the ratio λ of skin to muscle strain energies during elongation,

$$\lambda = \frac{\text{Energy}_S}{\text{Energy}_M} = \frac{E_S V_S}{E_M V_M}, \quad [11]$$

where E_S and E_M are Young's modulus of skin and muscle, respectively. The volume of the skin V_S and volume of the muscle V_M of a trunk segment of length ℓ may be written as

$$V_S = \frac{\pi\ell}{3}((R_1^2 + R_1 R_2 + R_2^2) - (\gamma_1^2 + \gamma_1\gamma_2 + \gamma_2^2) \quad [12]$$

$$V_M = \frac{\pi\ell}{3}((\gamma_1^2 + \gamma_1\gamma_2 + \gamma_2^2) - 2(r_1^2 + r_1 r_2 + r_2^2)), \quad [13]$$

respectively. The trunk segment is modeled as a frustum whose opposing faces are labeled with $i = 1, 2$. As shown in *SI Appendix*, Fig. S5, the cross-sectional radii of muscle and skin are R_i, skin thickness t_i, the nostril radius r_i, and the radius of the muscle without the skin $\gamma_i = R_i - t_i$.

Materials and Methods

Experiments with two African bush elephants (*Loxodonta africana*) were conducted at the Elephant Center at Zoo Atlanta over 2-h periods during the summer and fall of 2020 under the supervision of Zoo Atlanta staff. The two elephants included a 30-y-old male with a mass of 4,550 kg and a 37-y-old female elephant with a mass of 3,400 kg.

The elephants learned to reach a food incentive placed on top of two plastic boxes (each box with dimensions 61 × 61 × 61 cm). Keepers trained the elephants to reach the food over several weeks in the summer of 2020 until an 80% success rate was achieved. A black tarp provided a uniform background to facilitate filming. The boxes were placed at a distance of 200 cm from the edge of the elephant complex during data collection.

The elephant reaching motion was tracked with a high-speed monochrome camera (Phantom M11x) at 124 frames per second. The elephant keepers chose food incentives based on the elephant's liking, including grain pellets, apples, and celery. All experiments conducted with the elephants were voluntary. If the elephants did not participate, the testing day was concluded.

Digital Image Correlation Analysis and Curvature. Each elongation video was trimmed to include only the horizontal elongation of the trunk, which lasted between 200 and 300 individual frames. Image processing was performed using the Phantom Camera Control Application (PCC 3.5). Digital Image Correlation (DIC), a MATLAB software, was used to analyze the trunk's axial and lateral strain from the video data (44). A tracking grid ranging between 24 and 30 digital points was placed along the trunk to track the movement of the appendage across each video frame. Tracker points were manually placed along the trunk in 8.4- to 10.5-cm intervals, depending on the length of the trunk and its initial position. To measure curvature, we tracked two rows of 12 to 15 equally distanced points along the elephant trunk. We used a MATLAB curvature function (supplement in ref. 45) to determine the curvature of the dorsal and ventral sections. Raw video files and tracking data is included in the ASchulz19 repo.

Elephant Trunk Skin and Muscle Anatomy. The trunk was obtained from an elephant necropsy in 2011 conducted by the National Museum of Natural History (NMNH) at the Smithsonian Institution Osteoprepatory Laboratory (Suitland, MD). The proximal segment of the trunk (near the head), whose length was approximately one-third that of the trunk, was still attached to the skull and was dissected separately. The remaining two-thirds of the trunk was severed from the head and stored frozen at NMNH as *Loxodonta* specimen no. 590941. This trunk specimen was thawed and further dissected in 2015 and then sectioned into smaller units. The distal end (near the trunk tip) was flattened and desiccated and was immersed in water in an attempt to rehydrate. The trunk segments were then transferred in 2015 to the Center for Anatomy and Functional Morphology, Icahn School of Medicine (ISMMS, NY), where they were refrozen and stored at −15 °C. In July 2016, the segments were thawed and subsectioned for further anatomical analysis. The trunk sections (some frozen, some thawed) were CT scanned in 2018 in the Translational and Molecular Imaging Institute of ISMMS. The distal tip of the trunk was loaned to Georgia Tech for strain analyses. The trunk was rethawed in 2019 for further dissection at ISMMS, and skin samples were taken from the proximal end (as the distal end was desiccated) and sent to Georgia Tech for further analysis. The elephant's body weight before death was ∼4,000 kg. This elephant was a 38-y-old female elephant, which is close to the 3,400-kg 37-y-old female elephant filmed in our study. The trunk was also thawed and refrozen to be CT scanned in 2018. The original specimen was somewhat desiccated at the distal end, and therefore we took two samples from the proximal end to compare skin responses.

In March of 2019, portions of the frozen trunk were thawed to dissect the skin. Dissection occurred at Icahn School of Medicine at Mount Sinai before dissected samples were refrozen. Images of the samples precut can be seen in Fig. 4 *A* and *B*. We analyzed two skin samples in this paper. One was taken from the dorsal section and one from the ventral section. Both samples were 110 cm from the distal tip of the trunk. These samples were shipped to Imperial College London by the Smithsonian Institute Collections Department as a scientific exchange between the two CITES (the Convention on International Trade in Endangered Species of Wild Fauna and Flora) registered institutions in a dry-ice environment. Shipment of the tissue was approved by Animal Plant and Health Agency authorization no. ITIMP19.0822. The samples were stored at Imperial College London at 80° C until fixing and tensile testing in January of 2020.

A sample was dissected from each of the dorsal and ventral sections. Both dissected pieces were taken 110 cm from the tip of the trunk. Samples were cut to the dimensions of 6 × 2 for uniaxial stress testing to get as close as possible to American Society of Testing Materials (ASTM) standards (46). These length and width measurements reflect the skin in its natural or relaxed state, where the wrinkles and folds were not stretched or flattened. The samples were thawed, and the dermis was soaked in phosphate buffer solution (PBS). Connection points on the proximal and distal portions of each sample were made with barbless eyed hooks (Maver MT 7 size 10), as has been done with other tissue tensile tests (47–50). For loading, each sample was loaded for two trials consisting of three cycles each at a rate of 1 mm/s until a peak force of 3 kgf was achieved (Movie S5).

Images of a trunk cross-section were examined to quantify differences in the muscular structure of the dorsal and ventral portions of the trunk. Images were taken from four axial positions along the trunk, resulting in four separate cross-sectional images. Image segmentation was manually conducted to create shape overlays of the three muscle groups present in the trunk, including longitudinal, radial, and oblique muscles. This image segmentation was done for each muscle group individually and the entire trunk cross-section to allow us to discretize the overall cross-sectional image into the different muscle groups. After creating the muscle overlays an Adobe Illustrator script was employed to calculate the area of each overlay (51). Dividing each muscle group area by the total cross-sectional area resulted in the proportion of each muscle group present in the trunk cross-section (Fig. 4*D*). The sum of these proportions of cross-sections of muscle do not total to one as they do not account for the octopus nerve cord, and the elephant nostrils and a nerve cord.

Data Availability. We have included MATLAB files for the DIC of elephants, raw elephant elongation trials, and data spreadsheets of strain tracking available for download at the following repository: Zenodo (10.5281/zenodo.5780107) (52).

ACKNOWLEDGMENTS. We thank N. Elgart at Zoo Atlanta for assisting with elephant experiments. We thank J. Mendelson and the Georgia Tech Center for Education Integrating Science, Mathematics, and Computing (CEISMC) office, including H. Turcotte, Y. Kim, and M. Helms for supporting this project. We thank the Zoo Atlanta elephant keepers for their assistance in performing experiments with the elephants. We thank Dr. Ali Nabaviziadeh for arranging the collaboration with Dr. Reidenberg. We thank the imaging time donated by Dr. Cheuk Tang's group at Icahn School of Medicine at Mount Sinai. We thank J. Ososky, D. Lunde, and the Smithsonian Institution Museum of Natural History for their assistance with information regarding the frozen elephant trunk as well as loaning the elephant trunk to Icahn School of Medicine at Mount Sinai. D.L.H. and A.K.S. were supported by the US Army Research Laboratory and the US Army Research Office Mechanical Sciences Division, Complex Dynamics and Systems Program, under contract number W911NF-12-R-0011. M.B. was supported by a President's Undergraduate Award at Georgia Tech. S.S. was supported by Army Research Office Undergraduate Research Apprenticeship Program (URAP).

1. T. T. Hoang, P. T. Phan, M. T. Thai, N. H. Lovell, T. N. Do, Bio-inspired conformable and helical soft fabric gripper with variable stiffness and touch sensing. *Adv. Mater. Technol.* **5**, 2000724 (2020).
2. H. Tsukagoshi, A. Kitagawa, M. Segawa, "Active hose: An artificial elephant's nose with maneuverability for rescue operation" in *Proceedings 2001 ICRA. IEEE International Conference on Robotics and Automation (Cat. No.01CH37164)*, B. H. Lee, Ed. (IEEE, Seoul, South Korea, 2001), vol. 3, pp. 2454–2459.
3. M. Hannan, I. Walker, "The 'elephant trunk' manipulator, design and implementation" in *2001 IEEE/ASME International Conference on Advanced Intelligent Mechatronics. Proceedings (Cat. No.01TH8556)*, T.-J. Tarn, Ed. (IEEE, Como, Italy, 2001), vol. 1, pp. 14–19.
4. M. W. Hannan, I. D. Walker, Kinematics and the implementation of an elephant's trunk manipulator and other continuum style robots. *J. Robot. Syst.* **20**, 45–63 (2003).
5. R. J. Webster, B. A. Jones, Design and kinematic modeling of constant curvature continuum robots: A review. *Int. J. Robot. Res.* **29**, 1661–1683 (2010).
6. C. Majidi, Soft robotics: A perspective–Current trends and prospects for the future. *Soft Robotics* **1**, 5–11 (2014).
7. D. Trivedi, C. D. Rahn, W. M. Kier, I. D. Walker, Soft robotics: Biological inspiration, state of the art, and future research. *Appl. Bionics Biomech.* **5**, 99–117 (2008).
8. S. Tiefeng, Z. Libin, D. Mingyu, Y. Qinghua, Fruit harvesting continuum manipulator inspired by elephant trunk. *Biol. Eng.* **8**, 7 (2015).

9. W. Yang *et al.*, Natural flexible dermal armor. *Adv. Mater.* **25**, 31–48 (2013).
10. J. Choi *et al.*, Artificial stretchable armor for skin-interfaced wearable devices and soft robotics. *Extreme Mech. Lett.* **50**, 101537 (2022).
11. M. W. M. Tan, G. Thangavel, P. S. Lee, Rugged soft robots using tough, stretchable, and self-healable adhesive elastomers. *Adv. Funct. Mat.* **31**, 2103097 (2021).
12. A. Rafsanjani, Y. Zhang, B. Liu, S. M. Rubinstein, K. Bertoldi, Kirigami skins make a simple soft actuator crawl. *Sci. Robot.* **3**, eaar7555 (2018).
13. R. Truby, C. Della Santina, D. Rus, Distributed proprioception of 3D configuration in soft, sensorized robots via deep learning. *IEEE Robot. Autom. Lett.* **5**, 3299 –3306 (2020).
14. W. M. Kier, K. K. Smith, Tongues, tentacles and trunks: The biomechanics of movement in muscular-hydrostats. *Zool. J. Linn. Soc.* **83**, 307–324 (1985).
15. H. Omura, Osteology of pygmy blue whale with additional information on external and other characteristics. *Sci. Rep. Whales Res. Inst.* **22**, 1–27 (1970).
16. T. Kubodera, K. Mori, First-ever observations of a live giant squid in the wild. *Proc. Biol. Sci.* **272**, 2583–2586 (2005).
17. T. M. Williams, Heat transfer in elephants: Thermal partitioning based on skin temperature profiles. *J. Zool.* **222**, 235–245 (1990).
18. A. F. Martins *et al.*, Locally-curved geometry generates bending cracks in the African elephant skin. *Nat. Commun.* **9**, 3865 (2018).
19. N. M. Weissenböck, C. M. Weiss, H. M. Schwammer, H. Kratochvil, Thermal windows on the body surface of African elephants (Loxodonta africana) studied by infrared thermography. *J. Therm. Biol.* **35**, 182–188 (2010).
20. C. V. Anderson, T. Sheridan, S. M. Deban, Scaling of the ballistic tongue apparatus in chameleons. *J. Morphol.* **273**, 1214–1226 (2012).
21. S. Emura, T. Okumura, H. Chen, Morphology of the lingual papillae in the giraffe. *Okajimas Folia Anat. Jpn.* **89**, 99–103 (2013).
22. S. Hanassy, A. Botvinnik, T. Flash, B. Hochner, Stereotypical reaching movements of the octopus involve both bend propagation and arm elongation. *Bioinspir. Biomim.* **10**, 035001 (2015).
23. O. O. Igado, Gross morphometric study of the eyeball and tongue of the Nigerian local dog. *Ital. J. Anat. Embryol.* **116**, 104–110 (2011).
24. A. C. Noel, D. L. Hu, The tongue as a gripper. *J. Exp. Biol.* **221**, jeb176289 (2018).
25. P. M. Reis, S. Jung, J. M. Aristoff, R. Stocker, How cats lap: Water uptake by Felis catus. *Science* **330**, 1231–1234 (2010).
26. A. Harrison, Comparative osteology: A cross-species study of first rib parameters and their relation to body mass with emphasis on the woolly mammoth. *Am. J. Biomed. Sci. Res.* **3**, 340–346 (2019).
27. W. M. Kier, The diversity of hydrostatic skeletons. *J. Exp. Biol.* **215**, 1247–1257 (2012).
28. W. Kier, J. Leeuwen, A kinematic analysis of tentacle extension in the squid Loligo pealei. *J. Exp. Biol.* **200**, 41–53 (1997).
29. J. F. Wilson, U. Mahajan, S. A. Wainwright, L. J. Croner, A continuum model of elephant trunks. *J. Biomech. Eng.* **113**, 79–84 (1991).
30. W. M. Kier, M. P. Stella, The arrangement and function of octopus arm musculature and connective tissue. *J. Morphol.* **268**, 831–843 (2007).
31. X. Liang, S. A. Boppart, Biomechanical properties of in vivo human skin from dynamic optical coherence elastography. *IEEE Trans. Biomed. Eng.* **57**, 953–959 (2010).
32. A. Dąbrowska *et al.*, The relationship between skin function, barrier properties, and body-dependent factors. *Skin Res. Technol.* **24**, 165–174 (2018).
33. T. McMahon, Size and shape in biology. *Science* **179**, 1201–1204 (1973).
34. D. E. Moulton, T. Lessinnes, S. O'Keeffe, L. Dorfmann, A. Goriely, The elastic secrets of the chameleon tongue. *Proc. R. Soc. Math. Phys. Eng. Sci.* **472** (2016).
35. J. Zhao, S. Yan, J. Wu, Critical structure for telescopic movement of honey bee (Insecta: Apidae) abdomen: Folded intersegmental membrane. *J. Insect Sci.* **16**, 79 (2016).
36. H. L. More *et al.*, Scaling of sensorimotor control in terrestrial mammals. *Proc. Biol. Sci.* **277**, 3563–3568 (2010).
37. H. Marvi, J. Bridges, D. L. Hu, Snakes mimic earthworms: Propulsion using rectilinear travelling waves. *J. R. Soc. Interface* **10**, 20130188 (2013).
38. A. K. Schulz *et al.*, Suction feeding by elephants. *J. R. Soc. Interface* **18**, 20210215 (2021).
39. W. Kier, Hydrostatic skeletons and muscular hydrostats. *Nautilus* **8** (1992), pp. 206–208.
40. P. Dagenais, S. Hensman, V. Haechler, M. C. Milinkovitch, Elephants evolved strategies reducing the biomechanical complexity of their trunk. *Curr. Biol.* **31**, 4727–4737.e4 (2021).
41. M. M. Skinner *et al.*, Human evolution. Human-like hand use in Australopithecus africanus. *Science* **347**, 395–399 (2015).
42. L. Margheri, G. Ponte, B. Mazzolai, C. Laschi, G. Fiorito, Non-invasive study of Octopus vulgaris arm morphology using ultrasound. *J. Exp. Biol.* **214**, 3727–3731 (2011).
43. A. C. Noel, D. L. Hu, Cats use hollow papillae to wick saliva into fur. *Proc. Natl. Acad. Sci. U.S.A.* **115**, 12377–12382 (2018).
44. M. Senn, *Digital image correlation and tracking*. MATLAB Central File Exchange. (MATLAB 2018a, The MathWorks, Inc., Natick, MA, 2021).
45. D. J. Kroon, *2D line curvature and normals*. MATLAB Central File Exchange (MATLAB 2018a, The MathWorks, Inc., Natick, MA, 2021).
46. E28 Committee, "Test methods for tension testing of metallic materials" (Technical Report No. E8M-13a, ASTM International, West Conshohocken, PA, 2020).
47. M. Zemanek, J. Burša, M. Dětak, Biaxial tension tests with soft tissues of arterial wall. *Eng. Mech.* **16**, 3–11 (2008).
48. G. Sommer *et al.*, Multiaxial mechanical response and constitutive modeling of esophageal tissues: Impact on esophageal tissue engineering. *Acta Biomater.* **9**, 9379–9391 (2013).
49. G. M. Cooney, K. M. Moerman, M. Takaza, C. K. Simms, Uniaxial and biaxial mechanical properties of porcine linea alba. *J. Mech. Behav. Biomed. Mater.* **41**, 68–82 (2015).
50. Y. Lanir, Y. Fung, Two-dimensional mechanical properties of rabbit skin–II. Experimental results. *J. Biomech.* **7**, 171–182 (1974).
51. B. Buchanan, *GetShapeArea*. MATLAB Central File Exchange. (MATLAB 2018a, The MathWorks, Inc., Natick, MA, 2015).
52. A. Schulz *et al.*, Aschulz19/ElephantElongation: Elephant Elongation Reposity. Zenodo. https://zenodo.org/record/5780107#.YrnrUXbMLIU. Deposited 14 December 2021.